PHILOSOPHICAL MAGAZINE, 2018
VOL. 98, NO. 13, 1151–1169
https://doi.org/10.1080/14786435.2018.1431412

Taylor & Francis
Taylor & Francis Group

Influence of strain on dislocation core in silicon

L. Pizzagalli, J. Godet and S. Brochard

Departement of Physics and Mechanics of Materials, Pprime Institute, CNRS-Université de Poitiers UPR 3346, Chasseneuil Cedex, France

ABSTRACT

First principles, density functional-based tight binding and semi-empirical interatomic potentials calculations are performed to analyse the influence of large strains on the structure and stability of a 60° dislocation in silicon. Such strains typically arise during the mechanical testing of nanostructures like nanopillars or nanoparticles. We focus on bi-axial strains in the plane normal to the dislocation line. Our calculations surprisingly reveal that the dislocation core structure largely depends on the applied strain, for strain levels of about 5%. In the particular case of bi-axial compression, the transformation of the dislocation to a locally disordered configuration occurs for similar strain magnitudes. The formation of an opening, however, requires larger strains, of about 7.5%. Furthermore, our results suggest that electronic structure methods should be favoured to model dislocation cores in case of large strains whenever possible.

ARTICLE HISTORY
Received 19 October 2017
Accepted 17 January 2018

KEYWORDS
Dislocations; silicon; strain; density functional theory; tight binding; interatomic potential

1. Introduction

Covalent systems are characterised by strong and directional chemical bonds between atoms. Their mechanical behaviour is well known: stretched or bent materials first respond elastically, then yield by brittle fracture at relatively low deformation. Plastic deformation by dislocation motion only occurs at high temperature, or in dedicated experiments using a confining pressure preventing crack initiation and propagation [1,2]. This picture, valid for bulk systems, has been recently questioned when one or several system dimensions are reduced. Michler and co-workers reported the plastic deformation of gallium arsenide micropillars at room temperature [3,4]. Similar conclusions were made for silicon [5–7] and indium antimonide micropillars [8]. Furthermore, Gerberich and co-workers also observed the plastic deformation of silicon nanospheres [9,10] and nanocubes [11]. These results revealed a brittle to ductile transition as a function of the smallest dimension of the probed system [3–8,12–16], recently confirmed by molecular dynamics simulations [17].

The elastic regime also appears to be greatly extended when the dimension is reduced, with several investigations reporting very large strains prior to plastic

CONTACT L. Pizzagalli laurent.pizzagalli@univ-poitiers.fr

deformation [11,18–21]. This is especially true for stretched nanowires [18,20, 22,23], with measured elastic limits ranging from 5% to 13%. Wagner et al. also reported the elastic compression of silicon nanocubes up to 7% [11]. Such intriguing findings open the way for potential applications in strain engineering and nanoelectromechanics.

These large strains are likely to substantially influence the plastic deformation, and more specifically, the properties of dislocations. For instance, it has been shown that an hydrostatic compression of only 1–2% would sizeably alter the stability and mobility of a screw dislocation core in silicon [24]. Few studies also suggested that large strains can drastically modify dislocations properties [25–27]. Aside from these rare works, the influence of large strains, as encountered in nanosized systems, is usually overlooked, and a thorough investigation is critically lacking.

In this work, we investigate how large strains, up to 10% in tension or compression, change the structure and the stability of a dislocation core in a covalent material. We focus here, on silicon for the following reasons: (i) it is considered as the archetypal covalent material, (ii) it remains very important for technological applications and (iii) most of reported experiments on the mechanical properties of nanosized covalent systems concern silicon. At last, our knowledge of dislocation properties is better for silicon than for other covalent materials [28,29]. A 60° dislocation has been selected in our investigations, since this dislocation has been experimentally observed in severely deformed silicon nanowires at room temperature [30,31]. We considered five different initial core structures, simulated using different theoretical frameworks: density functional theory (DFT) [32,33], density functional-based tight binding (DFTB) [34] and three semi-empirical interatomic potentials. For each initial core configuration, we examined 11 strain states using DFT, the most accurate and expensive method, 41 with DFTB, and 441 with potentials. This large set of calculations allows us to analyse the influence of strain on the stability of a dislocation core with accuracy, and in particular to determine the thresholds corresponding to structural transformations in void opening and local disorder. Furthermore, we also evaluate the reliability of potentials to model silicon dislocations in these conditions.

The structure of the paper is as follows. First, a brief recall of the known core properties of the 60° dislocation in silicon is made. The models and the numerical simulation setups are then detailed. The results obtained using electronic structure approaches (DFT and DFTB), and potentials are reported in the next two sections. Finally, our findings are discussed in relation with the current state of the art.

2. 60° dislocation in silicon

Dislocations in silicon glide in {1 1 1} planes and are characterised by a Burgers vector equal to $a/2\langle 110\rangle$ (a being the lattice parameter). Due to the high lattice friction, they appear as straight segments lying in deep Peierls valleys, with screw and 60° orientations. Above the brittle to ductile transition temperature (around 900 °C), these dislocations are dissociated in 30° and 90° partials [35]. At low temperatures, roughly below the transition temperature, no dissociation is usually observed [28], although there are hints that partial dislocations could be active in specific cases [11].

The cubic diamond structure of silicon is characterised by two inequivalent families of {1 1 1} planes, historically called 'glide' and 'shuffle' [35]. High-temperature partial dislocations are located in 'glide' {1 1 1} planes. The situation is more complex for non-dissociated dislocations, for which several core configurations have been identified. In the case of the screw dislocation, the most stable core structure is located in 'glide' planes [36,37], but it is deemed that the active configuration for plastic deformation is a 'shuffle' core [38–40]. For the 60° dislocation, the lowest energy core is also located in 'glide' planes. However, it has not been detected in previous investigations, and it appears to be sessile [41]. Three other configurations, all located in 'shuffle' planes, have been identified [37]. The S1 core, represented in the Figure 1, is known for a long time [42] and is usually obtained from classical molecular dynamics simulations [43–47]. However, first principles calculations indicate that this configuration is not stable, and spontaneously relaxes to other structures, called S2 and S3 [41] (Figure 1). Unexpectedly, the same study also pointed that these two core structures are sessile too, hinting that the core S1, despite being unstable, is active during plastic deformation. For other covalent systems with cubic diamond, zinc blende or wurtzite structures, our knowledge is much scarce. However, we emphasise that the available information suggest that similar properties could be expected for these materials [29].

In this work, we aim at determining how large strains could affect the dislocation core stability. With its different possible core structures, the 60° dislocation is a good candidate. Furthermore, it has been shown to be active during the room temperature plastic deformation of nanostructures [17,30,31] and thin films [44,46]. A secondary objective is to investigate if strains could make the S1 core stable. Finally, it has been recently speculated that a 60° dislocation could be a precursor of a crack [48]. Our calculations should reveal whether an applied tension would eventually lead to breaking of bonds in the dislocation core, accounting for a possible nano-crack formation.

In our calculations, we first considered S1, S2 and S3 as initial configurations. S1 and S2 cores only differentiate by the bonds between atoms labelled i, j and k in Figure 1: a j–k bond (and no i–j bond) for S1, and a i–j bond (and no j–k bond) for S2. It is possible to generate two additional core configurations

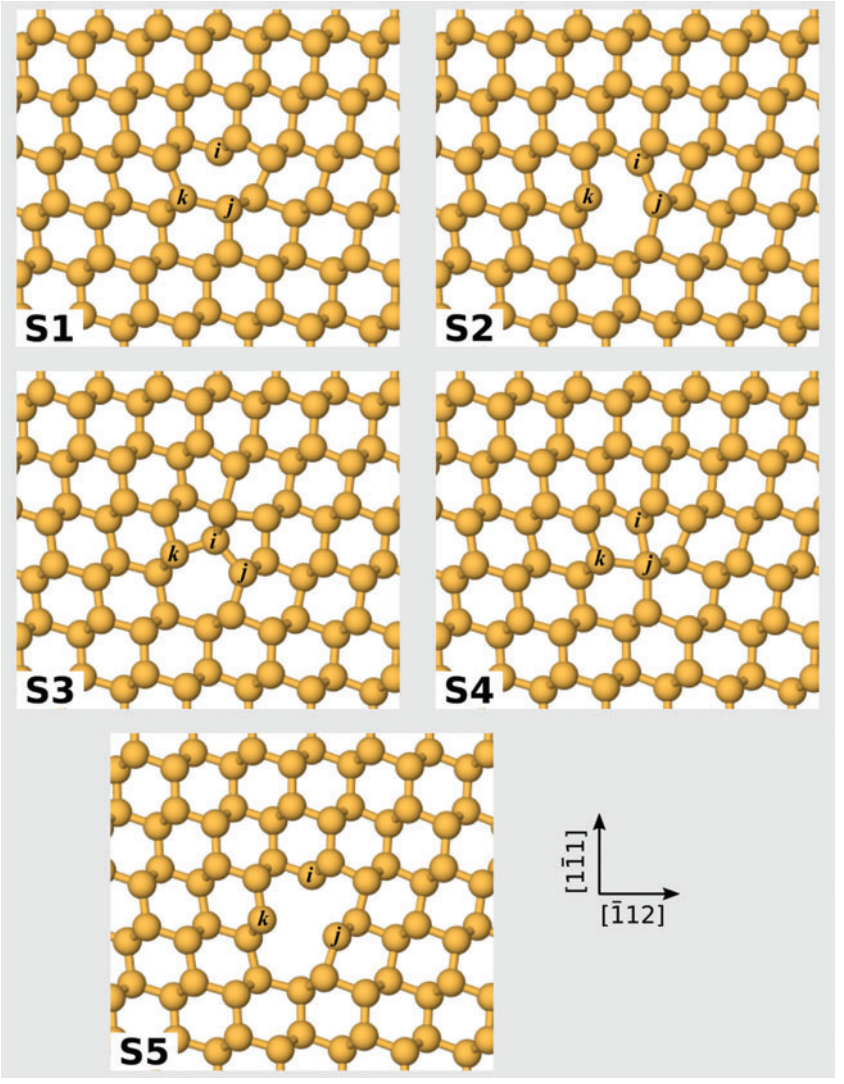

Figure 1. (colour online) 60° dislocation core configurations investigated in this work. The S1–S5 core structures can be easily identified by determining the presence of bonds between the atoms labelled *i*, *j* and *k* (see text for details). Two silicon atoms are considered bonded when their separation is lower than 2.85 Å.

with either two *i*–*j* and *j*–*k* bonds, or no bonds between *i*, *j* and *k* (Figure 1). These are respectively, called S4 and S5 hereinafter, to keep in line with the previous terminology [41]. S4 could be expected to be stable in compression, while S5 sounds like a small opening which may be energetically favoured in tension. Both S4 and S5 are also tested as initial configurations. Note that this classification is solely based on the topology of the dislocation core. For instance, two dislocation cores relaxed using DFT or a semi- empirical potential could be identified as S2, even with small differences in geometry. Finally, we do not take into account the 'glide' core G since it does not appear to be active during plastic

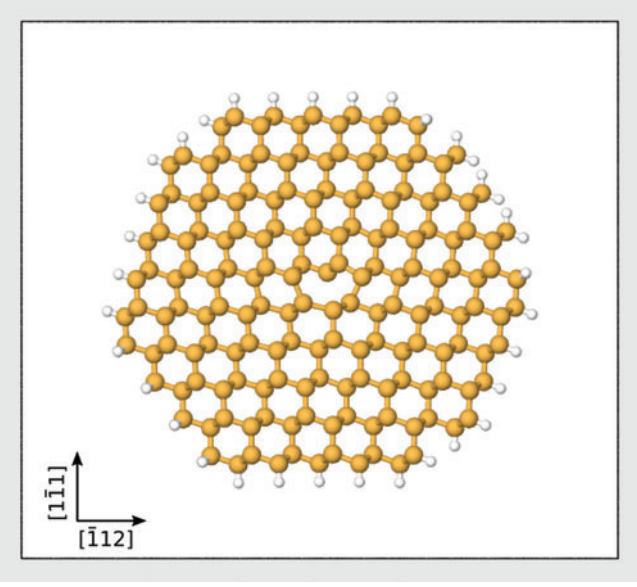

Figure 2. (colour online) Atomistic model used in the calculations (here, a S1 core configuration). The black frame shows the dimensions of the supercell along $\hat{x} = 1/\sqrt{6}[\bar{1}\,1\,2]$ and $\hat{y} = 1/\sqrt{3}[1\,\bar{1}\,1]$. The system is periodic along $\hat{z} = 1/\sqrt{2}[1\,1\,0]$, the out of the plane direction. Silicon atoms are shown as yellow spheres and hydrogen atoms (used to passivate Si surface atoms in electronic structure calculations) as white spheres. Two silicon atoms are considered bonded when their separation is lower than 2.85 Å.

deformation, and it is not possible to get 'shuffle' core structures transformed in G by a conservative displacement.

3. Numerical simulations methods

First principles calculations are performed using the DFT plane-wave code PWscf in the Quantum Espresso package [49,50]. The plane-wave cut-off is set to 20 Ry, which is a good compromise between the desired accuracy and the computational cost. It is an important issue here, due to the large set of computed cases, and the fact that the ionic structure relaxation of strained configurations requires an unusually high number of iterations to converge. The exchange and correlation contribution to the total energy is calculated using local density approximation (Perdew–Zunger), because it allows for an excellent description of the silicon 60° dislocation [41]. Furthermore, our preliminary tests show that it greatly improves the convergence of the electronic structure relaxation compared to generalised gradient approximations. We use projector augmented wave pseudopotentials in order to explicitly include only valence electrons in the calculations. With this setup, we compute a silicon lattice parameter $a = 5.4044$ Å and a bulk modulus equal to 99.5 GPa, in good agreement with experimental data. Due to the specific geometry of the dislocation model (detailed in the next section), electronic structure calculations are carried out using two k-points along the

dislocation line, generated with a $\frac{1}{2}$-shifted $(1 \times 1 \times 2)$ Monkhorst–Pack grid [51]. In case of highly strained configurations, we often find necessary to add an electron distribution smearing according to the Methfessel–Paxton method. At last, the ionic relaxation, performed using the Broyden–Fletcher–Goldfarb–Shanno algorithm, is considered achieved when the maximum force is below 10^{-2} eV Å^{-1}.

In addition to first principles calculations, we also performed self-consistent charge DFTB calculations. The DFTB+ code [52] and the Slater–Koster parameters in the *pbc-0.3* set [53–55] are used. The electronic structure is calculated with five k-points equally distributed along the dislocation line and a charge convergence criterion set to 10^{-5}. The maximum force criterion for ionic convergence using conjugate gradient is set to 10^{-3} eV Å^{-1}. The DFTB calculated lattice parameter is $a = 5.4597$ Å.

Finally, atomistic simulations are also performed with the LAMMPS code [56,57] and three different interatomic potentials, aiming at determining the most reliable one and also at assessing the influence of factors such as the small model size used in first principles calculations. Those are (i) an improved version of the Stillinger–Weber potential [58] ($a = 5.431$ Å), (ii) the Tersoff potential [59] ($a = 5.432$ Å) and (iii) a modified embedded atom method (MEAM) potential[1] [60] ($a = 5.417$ Å). These three potentials have already been used to describe the mechanical properties of silicon in earlier studies [58,60–62].

4. Numerical simulations models

To model dislocations in finite supercell, it is necessary to carefully deal with the long-range strain field that they generate [35]. Several methods are possible [29,63], among which we select the one where a single dislocation is introduced in a infinite cylinder, i.e. with periodicity along the dislocation line only. This allows for avoiding annihilation between dislocations, which could occur for the 60° dislocation. We first consider a large rectangular parallelepiped silicon crystal with the following orientations $\hat{x} = 1/\sqrt{6}[\bar{1}\,1\,2]$, $\hat{y} = 1/\sqrt{3}[1\,\bar{1}\,1]$ and $\hat{z} = 1/\sqrt{2}[1\,1\,0]$. The last axis corresponds to the dislocation line. A 'shuffle' 60° dislocation is generated in the crystal by displacing atoms according to anisotropic elasticity theory [64]. Different initial core configurations are obtained by slightly shifting the dislocation centre relative to the lattice, and by displacing selected core atoms by hand. We then cut a smaller piece of crystal, centered on the dislocation and with the geometry represented in the Figure 2. The final structure includes 336 silicon atoms, and is periodic along $\hat{z}$. The dimension along this axis is $2b$ ($b = a/\sqrt{2}$ is the Burgers vector norm), since it is needed for describing the reconstructed S3 core. It also allows for more freedom when relaxing deformed configurations. It is next embedded in a supercell of dimensions 45.16 Å $\times$ 41.53 Å $\times$ $\sqrt{2}a$, i.e. with vacuum in the $\hat{x}$ and $\hat{y}$ directions. This setup ensures a minimal separation of 9 Å between the model and periodic

images even when large tensile strains along $\hat{x}$ and $\hat{y}$ are investigated. Note that larger models have also been considered in interatomic potential calculations.

In the next step, the initial configuration given by elasticity theory is relaxed using the Tersoff potential, so as to obtain a stable core configuration. The final structure, represented in the Figure 2, corresponds to the S1 core. Note that during relaxation, and for all the calculations reported hereinafter, 106 silicon atoms in the two first surface layers are not allowed to relax. This scheme minimises the interaction between the surface and the dislocation core, in case of surface reconstruction for instance, and allows for a meaningful comparison of the different core energies. The other dislocation cores are obtained by manually displacing atoms in the core, followed by a second force relaxation. With the Tersoff potential, all the investigated core configurations are stable after relaxation. These configurations are then used as input for the other potential simulations and in electronic structure calculations, after an appropriate scaling accounting for the different lattice parameters.

In the case of electronic structure calculations, undercoordinated silicon surface atoms are also passivated with hydrogen atoms. Those are initially located at a distance of 1.494 Å which corresponds to the Si–H separation in a calculated SiH_4 molecule, and are allowed to move during relaxation. This procedure allows for a more efficient electronic structure relaxation.

The influence of a bi-axial strain along $\hat{x}$ and $\hat{y}$ is investigated. Practically, we apply a homogeneous strain on all atoms before force relaxation, the imposed deformation being conserved during relaxation thanks to the frozen surface atoms. A negative (positive) strain corresponds hereinafter to a compressive (tensile) state, respectively. The notation (−5%, 10%) indicates a strain state with a 5% compression along $\hat{x}$ and 10% tension along $\hat{y}$.

Our calculations allow us to determine (i) the relaxed core geometry from each initial structure (relative stability), (ii) the most stable core configuration amongst all of these (absolute stability), by comparing the total energies after relaxation for the same strain state. The outcome of these calculations is represented as stability maps (in Figures 3 and 5). The upper right quadrant corresponds to a bi-axial tension and the lower left one to bi-axial compression. The two other quadrants are strain states mixing compression and tension.

5. Electronic structure calculations

Figure 3 summarises the results of our DFT and DFTB calculations. Focusing first on the most stable geometry from DFT (upper left part of Figure 3), it appears that the S3 configuration is characterised by the lowest energy in the unstrained state, in agreement with our previous investigation [41]. We also find that both initial S2 and S3 structures converge to S3, while S1, S4 and S5 relax to S2, concurring with the reported metastability of S2 and the instability of S1. The energy difference of 1.29 eV b^{-1} between S2 and S3 is larger than previously

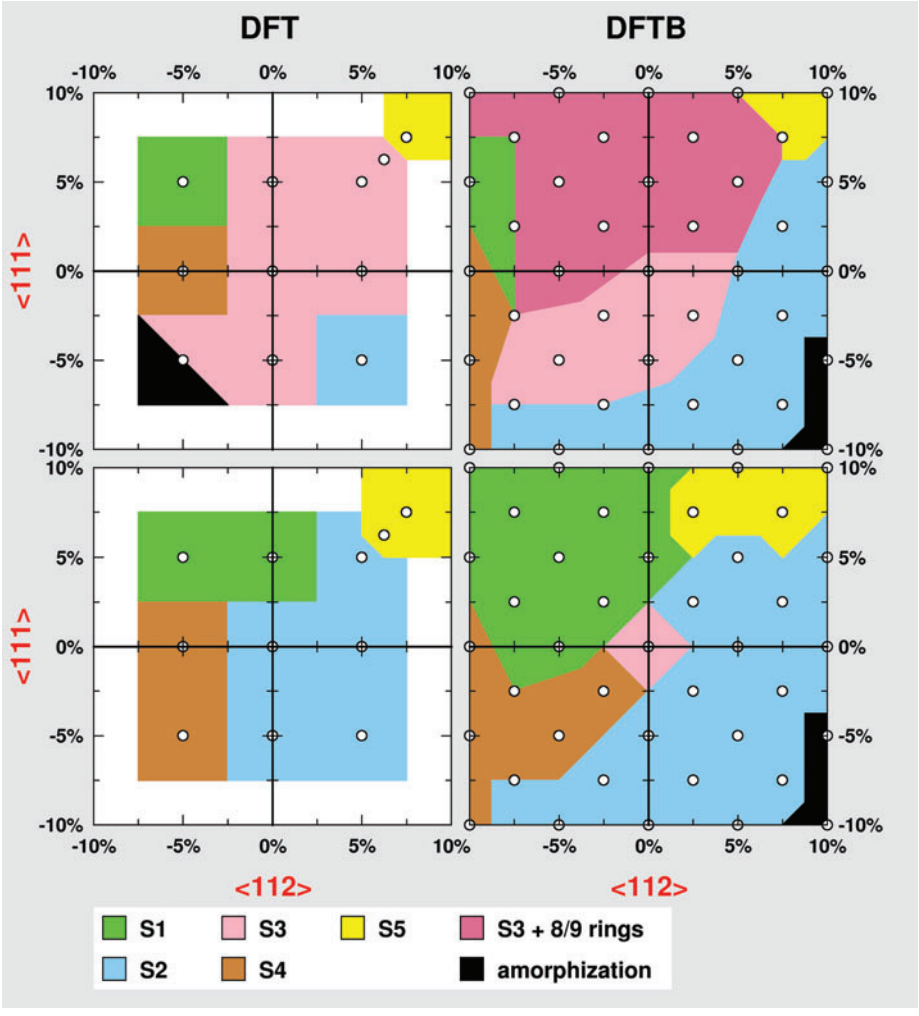

Figure 3. (colour online) Stability strain maps for DFT (left) and DFTB (right) calculations. Each white point corresponds to an investigated strain state. The colour code indicates the most stable structure amongst all calculated configurations (top), or the final structure after relaxation of an initial S1 configuration (bottom). The colour domains are drawn by interpolating the results of the calculations.

calculated [41]. S3 is also the most stable core in low strain conditions, especially for bi-axial tension. However, at (7.5%, 7.5%), it becomes energetically favourable to turn the dislocation core into a S5-like small opening, which is represented in Figure 4(a). The latter is obtained during relaxation when starting from S1, S2, S4 and S5 as initial configurations, with a final energy 0.76 eV b^{-1} lower than for the relaxed S3 core. Interestingly, for a slightly less strained state of (6.25%, 6.25%), an opening is also obtained from the same initial configurations, but the relaxed strained S3 core is now significantly more stable (with an energy difference equal to 0.45 eV b^{-1} in favour of S3). This suggests that the transition between an opening and a S3 core is sharp, and occurs in a narrow strain range.

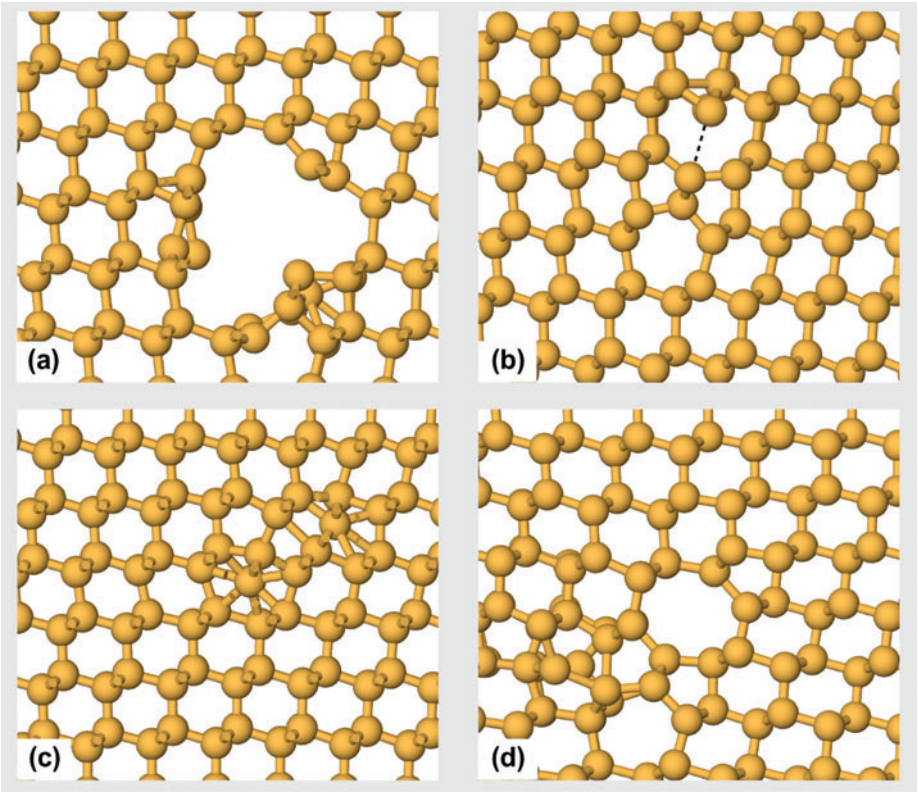

Figure 4. (colour online) Selected stable geometries after relaxation: (a) a S5-like opening obtained from DFT relaxation at (7.5%, 7.5%), (b) a specific geometry (noted 'S3+8/9 rings' in Figure 3) commonly obtained from DFTB relaxation and a tensile state along $\hat{y}$, (c, d) two final structures characterised by a local disorder obtained from DFT and (−5%, −5%), and DFTB and (10%, −10%), respectively. Two silicon atoms are considered bonded when their separation is lower than 2.85 Å.

DFT calculations also reveal that S2 becomes the most stable 60° dislocation core at (5%, −5%), the energy difference with the strained S3 being 0.15 eV b^{-1}. Conversely, at (5%, −5%), the S1 structure becomes energetically favoured, also with a small energy difference compared to S3 (0.09 eV b^{-1}). These two last results are consistent with the fact that a deformation along $\hat{x}$ will promote or prevent j–k bonding (Figure 1), whereas a deformation along $\hat{y}$ will affect i–j bonding. Following the same logic, one would expect an increased stability of S4 in case of bi-axial compression. This is indeed the case, S4 being obtained after relaxation of S1 and S4 initial configurations at (5%, −5%). However, an even lower energy is found for the configuration represented in Figure 4.c, obtained by relaxing an initial S5 configuration. The presence of highly coordinated atoms and distorted bonds is the fingerprint of a local disorder. This configuration is 0.19 eV b^{-1} lower than the S3 configuration. Nevertheless, a stable S4 configuration can be observed at (−5%, 0%), as the product of the relaxation of S1, S2, S4 or S5 initial configurations. The converged structure is characterised by an energy 0.25 eV b^{-1} lower than S3.

The outcome of DFTB calculations are reported in the upper right side of Figure 3. Since DFTB is less accurate than DFT, it is interesting to assess the reliability of these results. Comparing DFTB and DFT results, some similar trends can be observed, like the occurrence of S1, S2, S4 and S5 in roughly the same strain conditions. However, several differences appear also clearly. The most prominent one comes from a slightly different S3 geometry, represented in Figure 4(b), and called S3+8/9 rings in Figure 3. This configuration is obtained as the most stable state from the relaxation of an initial S3 core, mainly in the case of a tensile deformation along $\hat{y}$. Compared to S3, it is characterised by the formation of a eight- or nine-fold ring due to the rupture of a bond in the dislocation core (marked as a dashed line in Figure 4(b)). Another relevant feature is the lack of local amorphisation in bi-axial compression with DFTB, a preserved S4 core being the most stable structure even at $(-10\%, -10\%)$. Furthermore, a disordered state is obtained in case of large tension along $\hat{x}$ and compression along $\hat{y}$. For instance, the final geometry at $(-10\%, -10\%)$ is represented in Figure 4(d).

DFTB, like DFT, predicts a stable opening in case of bi-axial tensile strain, with approximately the same threshold. The strain domains associated with S1, S2 and S4 as being most stable states are also approximately in agreement, although for S1 and S4 they are shifted to larger compressive strains along $\hat{x}$. This is probably due to DFTB overrating the stability of S3 compared to DFT. In the case of S2, DFT predicts that it should be the most stable state in a wide range of strain states.

Bottom quadrants of Figure 3 also show stability strain maps obtained from both DFT and DFTB, but only from calculations with S1 as initial configuration. Those are especially interesting since S1 has been identified in previous investigations as the mobile 60° dislocation core [17,30,41,44,46]. The objective is here to investigate if a nucleated S1 dislocation core could turn into another, more stable, geometry depending on the strain conditions.

The analysis of these strain maps reveal that the two methods yield comparable results, except for a moderate compression along $\hat{x}$ and an unstrained state. For the latter, the DFT relaxation of S1 leads to the formation of S2, in agreement with previous works [41], whereas S3 is obtained using DFTB. Note that this is the only case where S3 is obtained from S1, probably because the bondings of the two configurations are too different, and a transformation requires significant displacements of atoms. Overall, these maps indicate that S2 is the most stable core in case of tension along $\hat{x}$ (except when combined with a high tension along $\hat{y}$), and in specific bi-axial compression conditions. Also, local amorphisation with DFT is not observed anymore, which would suggest that it is favoured by the complex S3 core geometry which already contains five-fold and seven-fold rings. Finally, only considering S1 as initial configuration allows for a slight increase of the stability domain of a stable S5 or even large opening, but large bi-axial tensile strains are still required.

6. Interatomic potential calculations

Thanks to a reduced computational cost, interatomic potential investigations can be performed on a finer grid of strain states compared to electronic structure calculations. Strains along $\hat{x}$ and $\hat{y}$ range from -10% to 10% with a step of 1%, leading to 441 possible bi-axial strain states, i.e. 2205 calculations for each potential. This large number motivates us to develop an automatic analysis of the final configurations. The identification of the different geometries was first based on the presence or not of bonds between atoms labelled i, j, and k in Figure 1. For instance, a S3 core includes k–i and i–j bonds, but no k–j bond. A covalent bond is assumed when the interatomic distance is equal or lower than 2.85 Å, since the electron density between two atoms has been shown to be negligible in amorphous silicon above this threshold [65,66]. In addition, the atoms coordination is calculated and used for further analysis. In case of several three-fold coordinated atoms, an opening is assumed to be present. With this criterion, a S5 geometry is considered as an opening. Also, a structure is tagged as locally disordered if there are at least two five-fold coordinated atoms. Finally, there are some cases for which the identification is not possible or ambiguous, because the final configuration largely departs from the initial one. This occurs for instance when the dislocation core moves during forces relaxation.

The results of the calculations and identification procedure are reported in Figure 5, for the three potentials. The comparison with Figure 3 reveals that the modified Stillinger–Weber potential roughly reproduces the DFT results for the most stable strained configuration, except for tension along $\hat{x}$ and compression along $\hat{y}$. In fact, with this potential, the S2 configuration is rarely the lowest energy configuration, unlike with DFT. The situation worsens when considering only S1 as initial configuration. S4 and to a lesser extent S1 then become favoured over large strain domains, still with no S2 configuration. Finally, in case of compressive strain greater than 7%, one often obtains not well defined structures, including local disorder for instance.

Conversely, the Tersoff potential always preserves the bonding of the initial configuration during the relaxation, allowing for an unambiguous identification of the final geometry. Also, the strain map for the most stable structure exhibits clear separated domains, in agreement with electronic structure calculations. However, it tends to favour both S4 and S5, compared to S1 and S3. The formation of openings would then be overestimated with the Tersoff potential. Analysing now the configurations obtained by relaxing a strained S1 core, one finds that the latter is stable except when a compressive strain greater than about 4% is applied along $\hat{y}$. This is consistent with the fact that the Tersoff potential overstate the strength of bonds, thus preventing the breaking of bonds during relaxation.

Using MEAM, we find that it is difficult to identify relaxed structures, especially in compression. Analysis of selected cases reveals that the final configurations are often messy, with a core transformation towards a locally disordered

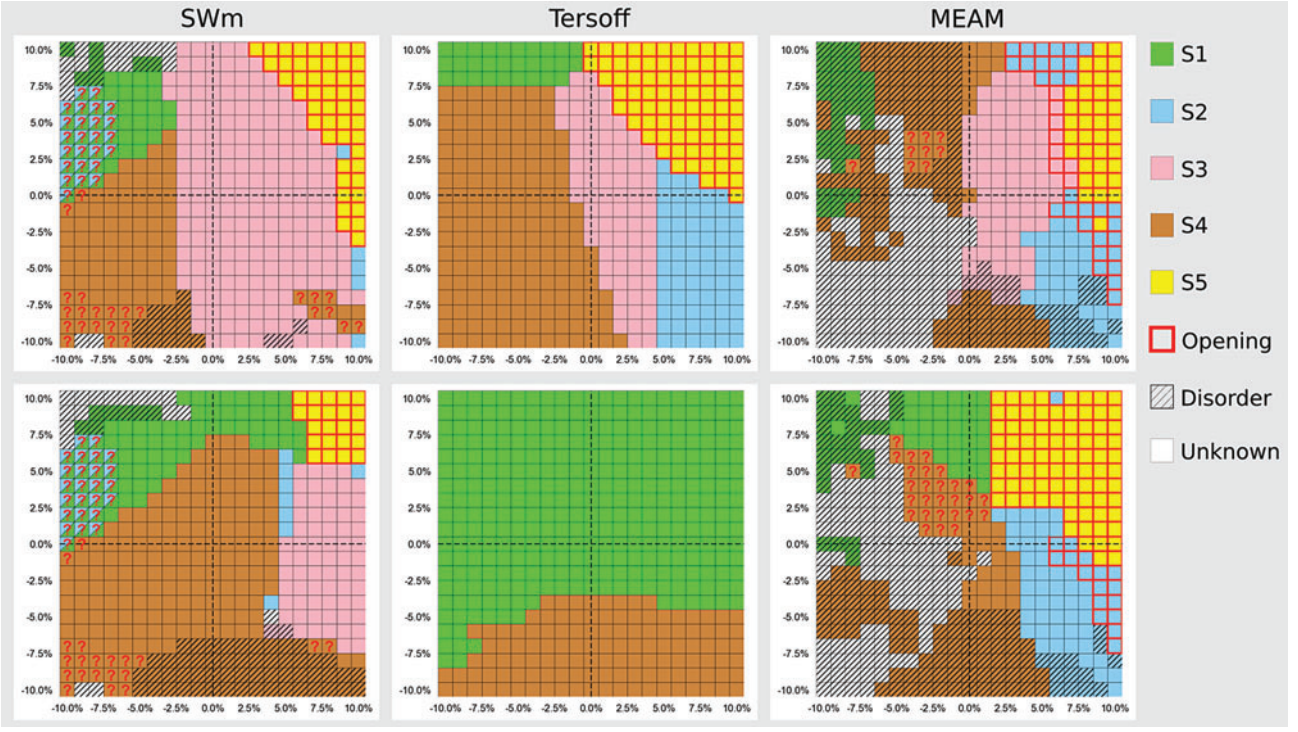

Figure 5. (colour online) Stability strain maps calculated using different interatomic potentials (Stillinger–Weber (SWm), Tersoff and MEAM). Top maps show the most stable structure amongst all calculated configurations, and the bottom ones the final structure after relaxation of an initial S1 configuration, analysed using the automatic analysis procedure explained in the text (colour code in the right side). Non-identified geometries are labelled as 'unknown', while a red question mark indicates that the geometry analysis was ambiguous. Finally, a dashed square signals the presence of a local disorder in the relaxed geometry.

state. However, in case of tension along $\hat{x}$, the most stable structure is in fair agreement with electronic structure calculations, reproducing the stability domains for S2, S3, and for openings. With an initial S1 core, this potential favours S2 in case of tension along $\hat{x}$ and compression along $\hat{y}$, like in DFT. However, it also overestimates S5, which is obtained even for small tensile strains along $\hat{x}$ and $\hat{y}$.

At last, interatomic potential calculations are also useful to check the validity of our computational model. First, we perform calculations to determine the most stable dislocation configurations within the same $\hat{x}$ and $\hat{y}$ strain ranges, but with a larger system. Results similar to those shown in Figure 5 are obtained, thus validating our computational setup. Second, we investigate the possible influence of the relaxation of the system along $\hat{z}$, i.e. the dislocation line. Here again, we find negligible differences compared to calculations described above.

7. Discussion

Our results all point to the same conclusion: the energetically most stable configuration for a 60° dislocation in silicon strongly depends on strain. All five investigated structures can be obtained. One may argue that these structures are topologically rather close, and that it does not greatly modify the properties of a 60° dislocation . This argument may hold true for S1 and S4, but not for the other configurations, which involve significant structural differences. For instance, the known transformation S2→S3 cannot be reversed [41]. This is also obvious by comparing a compact core like S1 with the stable distorted S5 geometry such as the one shown in Figure 4(a). Furthermore, we also predict that a moderate compressive state could lead to the transformation of the dislocation core into a locally disordered structure.

Focusing on the most reliable DFT data, we find that configurations S1, S2, and S4 could be more stable than S3 for strains of the order of 5%. Such levels can hardly be attained in bulk materials, even when using dedicated experiments. At low scale, though, similar or even greater strain magnitudes have been reported in several experiments [11,18,20–23], and our conclusions are then pertinent in this context. 5% is also the threshold in bi-axial compression above which a local disorder becomes energetically favoured. However, our calculations suggest that the formation of one opening directly from the dislocation core requires at least strain levels of about 7.5% in bi-axial tension. Such conditions might be encountered in highly stretched nanowires [18,22,23], but are probably too unusual to conclude that cracks could be directly initiated from a simple dislocation core in silicon.

Overall, we emphasise that it is difficult to assert that we have determined the most stable dislocation core for different strain conditions. This issue has been recognised as critical for a long time, in particular, for dislocations in covalent materials [29,37,67]. A common approach to generate an initial core structure is

to directly apply to atoms the displacements as given by elasticity theory, even if it is recognised that such a continuum theory cannot describe the non-elastic core. Different configurations can be obtained by shifting the dislocation centre relative to the crystal, and by subsequently displacing few selected core atoms. This is what we do here. But there is no guarantee that one does not miss the most stable structure. This issue is especially heightened in our work due to the presence of large strains. Using as initial configurations five stable structures first relaxed using the Tersoff potential, then strained, we try to explore as much as possible the configuration space, but we cannot exclude the hypothesis that unforeseen geometries might have lower energies.

In addition to investigating the most stable core configuration, we also examine a possible structural evolution of the S1 core geometry in presence of an applied strain. In fact, several studies have shown that this dislocation core plays an important role during the plastic deformation of silicon nanostructures. Comparing first to our previous work [41], its transient character is confirmed in the absence of strain, with a transformation to the S2 geometry. However, we also discover that it is possible to preserve a stable S1 configuration in specific strain conditions (tension along $\langle 1\,1\,1\rangle$, and compression along $\langle 1\,1\,2\rangle$). Besides, our investigations suggest that in case of bi-axial compression, S4 will become more stable than S1, which will probably be an intermediate state during dislocation motion. Finally, we show that the transformation of the S1 core into an opening would occur in case of bi-axial tension, for strain levels of about 6.5%.

Our calculations also allow for estimating the reliability of different theoretical frameworks in the specific situation of silicon dislocations under large strains. Assuming that DFT is the reference, we determine with no surprises that an electronic structure approach like DFTB is far superior to semi-empirical potentials. DFTB appears to be a good alternative to DFT, since it is reliable enough to qualitatively reproduce most of DFT results. Conversely, interatomic potentials are not very reliable, in particular, in case of compressive state. A better agreement is obtained for tensile states, but it remains qualitative at best.

It is tempting to compare the results reported above with those available in the literature, and in particular with experiments where the strain state is well characterised. Unfortunately, such a comparison is rather difficult in most cases. Indeed, here, we investigated bi-axial deformations along $\langle 1\,1\,1\rangle$ and $\langle 1\,1\,2\rangle$, the two canonical orientations for dislocations [35]. Only normal strains are then considered. In mechanically tested nanostructures, shear strains can be present, which have not been considered in the present work. Since it is unreasonable to investigate all possible strain states, the comparison with a specific experiment could be made only by performing calculations within the same strain conditions, if the latter are known. Note that the presence of shear strains could significantly complicate the theoretical investigations though, since it could lead to dislocation displacement during relaxation.

At last, we perform 0 K static calculations in this work, with conjugated gradients relaxation of forces. Nonetheless, the dynamical motion of dislocations is probably an important factor, that can influence the properties of dislocation. A known example is precisely the 60° dislocation in silicon, which we have shown to move with the S1 core although this core is not stable at rest [41]. Then, one could wonder whether dynamics will significantly preserve the geometry of a propagating dislocation core, by inertia, or if alternatively it will favour its transformation. An interesting analogy can be made with crack propagation in silicon, which depends on the fine structure of the crack tip, but also on the dynamics [68]. The use of approximate electronic structure calculations like DFTB, or of multiscale approaches [68], seems a good strategy for studying dynamical aspects since our investigations revealed that semi-empirical potentials are not well suited for describing dislocation cores in largely deformed states.

8. Conclusions

In this work, we investigate the influence of large strains on the structure and stability of a 60° dislocation in silicon, by performing electronic structure and semi-empirical potentials calculations. Such a study is especially needed since recent experimental advances at low scale allow for the mechanical deformation of covalent nanostructures at very large strains, although the properties of dislocations are usually studied without considering an applied strain.

We find out that the core structure strongly depends on the strain state, resulting in different geometries, for strain levels of about 5%. In compression, a dislocation core could also lead to a locally disordered state. Larger strains are however required for the dislocation core transformation into an opening. Our analyses also reveal that the transient character of the glissile S1 core is lost in case of appropriate strain conditions. Finally, a comparison of the different approaches suggests that semi-empirical interatomic potentials should be used with caution, because their reliability can be questionable for the description of highly strained dislocation cores. These results hint that future works should be aimed at investigating how large applied strains would influence the dynamics of dislocations.

Notes

1. The MEAM potential we use in this work is a slightly modified version of the potential published in Ref. [60], with the following parameters: $delr = 3.0$, $C_{\min} = 1.0$, $C_{\max} = 2.8$.

Disclosure statement

No potential conflict of interest was reported by the authors.

Funding

All calculations have been performed using the supercomputer facilities at the Spin Center at the University of Poitiers. The authors acknowledge the support of the French Agence Nationale de la Recherche (ANR), [grant ANR-12-BS04-0003] (project BIDUL).

References

[1] J. Rabier and J.L. Demenet, *Low temperature, high stress plastic deformation of semiconductors: The silicon case*, Phys. Stat. Sol. (b) 222 (2000), p. 63.
[2] B. Kedjar, L. Thilly, J.L. Demenet, and J. Rabier, *Plasticity of indium antimonide between −176 and 400 °C under hydrostatic pressure*, Part ii: Microscopic aspects of the deformation, Acta Mater. 58 (2010), p. 1426.
[3] J. Michler, K. Wasmer, S. Meier, F. Östlund, and K. Leifer, *Plastic deformation of gallium arsenide micropillars under uniaxial compression at room temperature*, Appl. Phys. Lett. 90 (2007), p. 043123.
[4] F. Östlund, P. Howie, R. Ghisleni, S. Korte, K. Leifer, W. Clegg, and J. Michler, *Ductile-brittle transition in micropillar compression of gaas at room temperature*, Philos. Mag. 91 (2011), p. 1190.
[5] F. Östlund, K. Rzepiejewska-Malyska, K. Leifer, L.M. Hale, Y. Tang, R. Ballarini, W.W. Gerberich, and J. Michler, *Nanostructure fracturing: Brittle-to-ductile transition in uniaxial compression of silicon pillars at room temperature*, Adv. Funct. Mater. 19 (2009), pp. 2439–2444.
[6] S. Korte, J. Barnard, R. Stearn, and W. Clegg, *Deformation of silicon - insights from microcompression testing at 25–500 °C*, Int. J. Plasticity 27 (2011), p. 1853.
[7] J. Rabier, A. Montagne, J.L. Demenet, J. Michler, and R. Ghisleni, *Silicon micropillars: High stress plasticity*, Phys. Stat. Sol. (c) 10 (2013), pp. 11–15.
[8] L. Thilly, R. Ghisleni, C. Swistak, and J. Michler, *In situ deformation of micro-objects as a tool to uncover the micro-mechanisms of the brittle-to-ductile transition in semiconductors: the case of indium antimonide*, Philos. Mag. 92 (2012), pp. 3315–3325.
[9] J. Deneen, W. Mook, A. Minor, W. Gerberich, and C. Barry, *Carter, In situ deformation of silicon nanospheres*, J. Mater. Sci. 41 (2006), pp. 4477–4483.
[10] W.M. Mook, J.D. Nowak, C.R. Perrey, C.B. Carter, R. Mukherjee, S.L. Girshick, P.H. McMurry, and W.W. Gerberich, *Compressive stress effects on nanoparticle modulus and fracture*, Phys. Rev. B 75 (2007), p. 214112. doi:10.1103/PhysRevB.75.214112.
[11] A.J. Wagner, E.D. Hintsala, P. Kumar, W.W. Gerberich, and K.A. Mkhoyan, *Mechanisms of plasticity in near-theoretical strength sub-100 nm si nanocubes*, Acta Mater. 100 (2015), pp. 256–265. Available at http://www.sciencedirect.com/science/article/pii/S1359645415006060.
[12] A. Beaber, J. Nowak, O. Ugurlu, W. Mook, S. Girshick, R. Ballarini, and W. Gerberich, *Smaller is tougher*, Philos. Mag. 91 (2011), pp. 1179–1189. doi:10.1080/14786435.2010.487474.
[13] W.W. Gerberich, D.D. Stauffer, A.R. Beaber, and N.I. Tymiak, *A brittleness transition in silicon due to scale*, J. Mater. Res. 27 (2012), pp. 552–561.
[14] W. Kang and M.T.A. Saif, *In situ study of size and temperature dependent brittle-to-ductile transition in single crystal silicon*, Adv. Funct. Mater. 23 (2013), pp. 713–719.
[15] B.N. Jaya, J.M. Wheeler, J. Wehrs, J.P. Best, R. Soler, J. Michler, C. Kirchlechner, and G. Dehm, *Microscale fracture behavior of single crystal silicon beams at elevated temperatures*, Nanoletters 16 (2016), pp. 7597–7603.

[16] E.D. Hintsala, S. Bhowmick, X. Yueyue, R. Ballarini, S.A.S. Asif, and W.W. Gerberich, *Temperature dependent fracture initiation in microscale silicon*, Superlatt. Microstruc. 130 (2017), pp. 78–82.
[17] F. Abed El Nabi, J. Godet, S. Brochard, and L. Pizzagalli, *Onset of ductility and brittleness in silicon nanowires mediated by dislocation nucleation*, Model. Simul. Mater. Sc. 23 (2015), p. 025010. Available at http://stacks.iop.org/0965-0393/23/i=2/a=025010.
[18] Y. Zhu, F. Xu, Q. Qin, W.Y. Fung, and W. Lu, *Mechanical properties of vapor-liquid-solid synthesized silicon nanowires*, Nanoletters 9 (2009), pp. 3934–3939. doi:10.1021/nl902132w.
[19] F. Ureña, S.H. Olsen, L. Šiller, U. Bhaskar, T. Pardoen, and J.P. Raskin, *Strain in silicon nanowire beams*, J. Appl. Phys. 112 (2012), p. 114506. Available at http://scitation.aip.org/content/aip/journal/jap/112/11/10.1063/1.4765025.
[20] D.M. Tang, C.L. Ren, M.S. Wang, X. Wei, N. Kawamoto, C. Liu, Y. Bando, M. Mitome, N. Fukata, and D. Golberg, *Mechanical properties of si nanowires as revealed by in situ transmission electron microscopy and molecular dynamics simulations*, Nanoletters 12 (2012), p. 1898.
[21] R. Shao, K. Zheng, Y. Zhang, Y. Li, Z. Zhang, and X. Han, *Piezoresistance behaviors of ultra-strained sic nanowires*, Appl. Phys. Lett. 101 (2012), p. 233109.
[22] T. Kizuka, Y. Takatani, K. Asaka, and R. Yoshizaki, *Measurements of the atomistic mechanics of single crystalline silicon wires of nanometer width*, Phys. Rev. B 72 (2005), p. 035333.
[23] H. Zhang, J. Tersoff, S. Xu, H. Chen, Q. Zhang, K. Zhang, Y. Yang, C.S. Lee, K.N. Tu, J. Li, and Y. Lu, *Approaching the ideal elastic strain limit in silicon nanowires*, Sci. Adv. 2 (2016), p. e1501382.
[24] L. Pizzagalli, J.L. Demenet, and J. Rabier, *Theoretical study of pressure effect on the dislocation core properties in semiconductors*, Phys. Rev. B 79 (2009), p. 045203.
[25] J. Amodeo, P. Carrez, and P. Cordier, *Modelling the effect of pressure on the critical shear stress of mgo single crystals*, Philos. Mag. 92 (2012), pp. 1523–1541.
[26] Z. Li and R. Picu, *Shuffle-glide dislocation transformation in si*, J. Appl. Phys. 113 (2013), p. 083519.
[27] Z. Li, N. Mathew, and R. Picu, *Dependence of peierls stress on lattice strains in silicon*, Comput. Mat. Sci. 77 (2013), pp. 343–347. Available at http://www.sciencedirect.com/science/article/pii/S0927025613002565.
[28] J. Rabier, L. Pizzagalli, and J.L. Demenet, *Dislocations in silicon at high stress*, in *Dislocation in Solids*, chap. 93, Vol. 16, L. Kubin and J.P. Hirth, eds., Elsevier, Amsterdam, 2010, p. 47.
[29] D. Rodney, L. Ventelon, E. Clouet, L. Pizzagalli, and F. Willaime, *Ab initio modeling of dislocation core properties in metals and semiconductors*, Acta Mater. 124 (2017), pp. 633–659.
[30] X. Han, K. Zheng, Y. Zhang, X. Zhang, Z. Zhang, and Z.L. Wang, *Low-temperature in situ large-strain plasticity of silicon nanowires*, Adv. Mater. 19 (2007), p. 2112.
[31] L. Wang, K. Zheng, Z. Zhang, and X. Han, *Direct atomic-scale imaging about the mechanisms of ultralarge bent straining in si nanowires*, Nanoletters 11 (2011), pp. 2382–2385.
[32] P. Hohenberg and W. Kohn, *Inhomogeneous electron gas*, Phys. Rev. 136 (1964), p. B864.
[33] W. Kohn and L.J. Sham, *Self-consistent equations including exchange and correlation effects*, Phys. Rev. 140 (1965), p. A1133.
[34] T. Frauenheim, G. Seifert, M. Elsterner, Z. Hajnal, G. Jungnickel, D. Porezag, S. Suhai, and R. Scholz, *A self-consistent charge density-functional based tight-binding method for*

predictive materials simulations in physics, chemistry and biology, Physica Status Solidi (b) 217 (2000), pp. 41–62.
[35] J.P. Hirth and J. Lothe, *Theory of Dislocations*, Wiley, New York, 1982.
[36] C.Z. Wang, J. Li, K.M. Ho, and S. Yip, *Undissociated screw dislocation in si: Glide or shuffle set?*, Appl. Phys. Lett. 89 (2006), p. 051910.
[37] L. Pizzagalli, J. Godet, J. Guénolé, and S. Brochard, *Dislocation cores in silicon: new aspects from numerical simulations*, J. Phys. Conf. Ser. 281 (2011), p. 012002.
[38] W. Cai, *Atomistic and mesoscale modeling of dislocation mobility*, Ph.D. diss, MIT, 2001.
[39] L. Pizzagalli, A. Pedersen, A. Arnaldsson, H. Jónsson, and P. Beauchamp, *Theoretical study of kinks on screw dislocation in silicon*, Phys. Rev. B 77 (2008), p. 064106.
[40] L. Pizzagalli and P. Beauchamp, *Dislocation motion in silicon: The shuffle-glide controversy revisited*, Philos. Mag. Lett. 88 (2008), p. 421.
[41] L. Pizzagalli, J. Godet, and S. Brochard, *Glissile dislocations with transient cores in silicon*, Phys. Rev. Lett. 103 (2009), p. 065505.
[42] J. Hornstra, *Dislocations in the diamond lattice*, J. Phys. Chem. Solids 5 (1958), p. 129.
[43] J. Godet, L. Pizzagalli, S. Brochard, and P. Beauchamp, *Theoretical study of dislocation nucleation from simple surface defects in semiconductors*, Phys. Rev. B 70 (2004), p. 054109.
[44] A. Marzegalli, F. Montalenti, and L. Miglio, *Stability of shuffle and glide dislocation segments with increasing misfit in ge/si$_{1-x}$ge$_x$(0 0 1) epitaxial layers*, Appl. Phys. Lett. 86 (2005), p. 041912.
[45] C. Li, Q. Meng, K. Zhong, and C. Wang, *Computer simulation of the* 60° *dislocation interaction with vacancy cluster in silicon*, Phys. Rev. B 77 (2008), p. 045211.
[46] J. Godet, P. Hirel, S. Brochard, and L. Pizzagalli, *Evidence of two plastic regimes controlled by dislocation nucleation in silicon nanostructures*, J. Appl. Phys. 105 (2009), p. 026104.
[47] S. Izumi, H. Ohta, C. Takahashi, T. Suzuki, and H. Saka, *Shuffle-set dislocation nucleation in semiconductor silicon device*, Philos. Mag. Lett. 90 (2010), pp. 707–714.
[48] J. Rabier, F. Pailloux, and L. Pizzagalli, *On the dislocation core structures associated to point defect cluster formation in diamond and silicon*, Phys. Stat. Sol. (c) 12 (2015), pp. 1067–1070.
[49] Available at Http://www.quantum-espresso.org/.
[50] P. Giannozzi, S. Baroni, N. Bonini, M. Calandra, R. Car, C. Cavazzoni, D. Ceresoli, G.L. Chiarotti, M. Cococcioni, I. Dabo, A. Dal Corso, S. de Gironcoli, S. Fabris, G. Fratesi, R. Gebauer, U. Gerstmann, C. Gougoussis, A. Kokalj, M. Lazzeri, L. Martin-Samos, N. Marzari, F. Mauri, R. Mazzarello, S. Paolini, A. Pasquarello, L. Paulatto, C. Sbraccia, S. Scandolo, G. Sclauzero, A.P. Seitsonen, A. Smogunov, P. Umari and R.M. Wentzcovitch, *Quantum espresso: A modular and open-source software project for quantum simulations of materials*, J. Phys. Condens. Matter 21 (2009), p. 395502. Available at http://www.quantum-espresso.org.
[51] H.J. Monkhorst and J.D. Pack, *Special points for brillouin-zone integrations*, Phys. Rev. B 13 (1976), p. 5188.
[52] B. Aradi, B. Hourahine, and T. Frauenheim, *Dftb+, a sparse matrix-based implementation of the dftb method*, J. Phys. Chem. A 111 (2007), pp. 5678–5684.
[53] Available at Https://www.dftb.org/.
[54] A. Sieck, *Structure and physical properties of silicon clusters and of vacancy clusters in bulk silicon*, Ph.D. diss., University of Paderborn, 2000.
[55] C. Koehler and T. Frauenheim, *Molecular dynamics simulations of cfx ($x = 2, 3$) molecules at si3n4 and sio2 surfaces*, Surf. Sci. 600 (2006), pp. 453–460.
[56] Available at Http://lammps.sandia.gov/.

[57] S. Plimpton, *Fast parallel algorithms for short-range molecular dynamics*, J. Comput. Phys. 117 (1995), pp. 1–19.
[58] L. Pizzagalli, J. Godet, J. Guénolé, S. Brochard, E. Holmstrom, K. Nordlund, and T. Albaret, *A new parametrization of the stillinger-weber potential for an improved description of defects and plasticity of silicon*, J. Phys. Condensed Matter. 25 (2013), p. 055801.
[59] J. Tersoff, *Modeling solid-state chemistry: Interatomic potentials for multicomponent systems*, Phys. Rev. B 39 (1989), p. 5566.
[60] J. Godet, C. Furgeaud, L. Pizzagalli, and M.J. Demkowicz, *Uniform tensile elongation in au-si core-shell nanowires*, Extreme Mech. Lett. 8 (2016), pp. 151–159. Available at http://www.sciencedirect.com/science/article/pii/S235243161630092X.
[61] V.V. Bulatov, J.F. Justo, W. Cai, S. Yip, A.S. Argon, T. Lenosky, M. de Koning, and T.D. de la Rubia, *Parameter-free modelling of dislocation motion: The case of silicon*, Philos. Mag. A 81 (2001), p. 1257.
[62] L. Pizzagalli, P. Beauchamp, and J. Rabier, *Undissociated screw dislocations in silicon: Calculations of core structure and energy*, Philos. Mag. A 83 (2003), p. 1191.
[63] V. Bulatov and W. Cai, *Computer simulations of dislocations*, Oxford Series on Materials Modelling. Oxford University Press, New York, 2006.
[64] A.N. Stroh, *Dislocations and cracks in anisotropic elasticity*, Philos. Mag. 3 (1958), p. 625.
[65] N. Bernstein, J.L. Feldman, and M. Fornari, *Structural model of amorphous silicon annealed with tight binding*, Phys. Rev. B 74 (2006), p. 205202.
[66] A. Pedersen, L. Pizzagalli, and H. Jónsson, *Optimal atomic structure of amorphous silicon obtained from density functional theory calculations*, New J. Phys. 19 (2017), p. 063018.
[67] V.V. Bulatov, *Bottomless complexity of core structure and kink mechanisms of dislocation motion in silicon*, Scripta Materialia 45 (2001), pp. 1247–1252. Available at http://www.sciencedirect.com/science/article/pii/S1359646201011575.
[68] D. Fernandez-Torre, T. Albaret, and A. De Vita, *Role of surface reconstruction in* (1 1 1) *silicon fracture*, Phys. Rev. Lett. 105 (2010), p. 185502.